

A warped $m = 2$ water maser disc in V778 Cyg?

Natalia Babkovskaia,^{1*} Juri Poutanen,¹ Anita M. S. Richards,² and Ryszard Szczerba³

¹*Astronomy Division, PO Box 3000, FIN-90014 University of Oulu, Finland*

²*Jodrell Bank Observatory, University of Manchester, Macclesfield, Cheshire SK11 9DL*

³*N. Copernicus Astronomical Center, Radańska 8, 87-100 Toruń, Poland*

3 October 2018

ABSTRACT

The silicate carbon star V778 Cyg is a source of 22 GHz water maser emission which was recently resolved by MERLIN. Observations revealed an elongated S-like structure along which the velocities of the maser features show a linear dependence on the impact parameter. This is consistent with a doubly-warped $m = 2$ disc observed edge-on. Water masers and silicate dust emission (detected by *IRAS* and *ISO*) have a common origin in O-rich material and are likely to be co-located in the disc. We propose a detailed self-consistent model of a masing gas-dust disc around a companion to the carbon star in a binary system, which allows us to estimate the companion mass of $1.7 \pm 0.1 M_{\odot}$, the disc radius of 40 ± 3 AU and the distance between companions of ~ 80 AU. Using a dust-gas coupling model for water masing, we calculate the maser power self-consistently, accounting for both the gas and the dust energy balances. Comparing the simulation results with the observational data, we deduce the main physical parameters of the masing disc, such as the gas and dust temperatures and their densities. We also present an analysis of the stability of the disc.

Key words: circumstellar matter – masers – stars: AGB and post-AGB – stars: carbon – stars: chemically peculiar – stars: binaries

1 INTRODUCTION

Carbon stars with amorphous silicate dust features at 10 and 18 μm (silicate carbon stars) which typify O-rich dust envelopes (Little-Marenin 1986), were first discovered with the *Infrared Astronomical satellite (IRAS)*. A distinguishing feature of this class of carbon stars is a mixed chemistry, i.e. simultaneous presence of O- and C-rich material around them. The *Infrared Space Observatory (ISO)* revealed that this mixed chemistry phenomenon is not unique. About 20 silicate carbon stars are known in our Galaxy (Chen et al. 1999; Szczerba 2002).

The best known example of this class is V778 Cyg. Infrared observations show that the shape and intensity of the silicate features in the spectrum of V778 Cyg did not change during a period of about 14 years (Yamamura et al. 2000, hereafter Y00). This indicates that the O-rich material is located in some stable configuration. Y00 proposed that it is stored in a disc around an invisible (most probably main-sequence) star, which is the companion of the carbon star in a binary system (see also Morris et al. 1987; Evans 1990; Barnbaum et al. 1991). V778 Cyg also shows H₂O and OH maser emission. Single dish monitoring of water maser emission during 12 years shows a very small velocity shift ($< 0.5 \text{ km s}^{-1}$)

of the main components in the maser spectrum (Engels & Leinert 1994)¹.

In October 2001 water maser emission from V778 Cyg was imaged using five telescopes of MERLIN (Szczerba et al. 2006). The position of the maser complex was found to be displaced by ~ 190 mas from the position of the C-star measured 10 years previously, which is unlikely to be a result of the proper motion. Instead, this can be considered as an additional evidence that the O-rich material is stored around the secondary (Szczerba et al. 2006).

The MERLIN data show that the masers are distributed in an S-shaped figure. In this paper, we construct a model of the spatial and velocity distribution of the water masers around V778 Cyg. We develop a self-consistent description of the physical mechanism of the water maser pumping together with an explanation for the observed infrared silicate dust emission. We also determine the main parameters of the system.

We present the main observational data in Section 2. We model the 22-GHz water maser spatial and velocity distributions and the infrared dust emission as well as the physical mechanism of maser pumping in Section 3. We discuss our results in Section 4 and conclude in Section 5.

* E-mail: natalia.babkovskaia@oulu.fi (NB)

¹ see also <http://www.hs.uni-hamburg.de/DE/Ins/Per/Engels/engels/wcatalog.html>

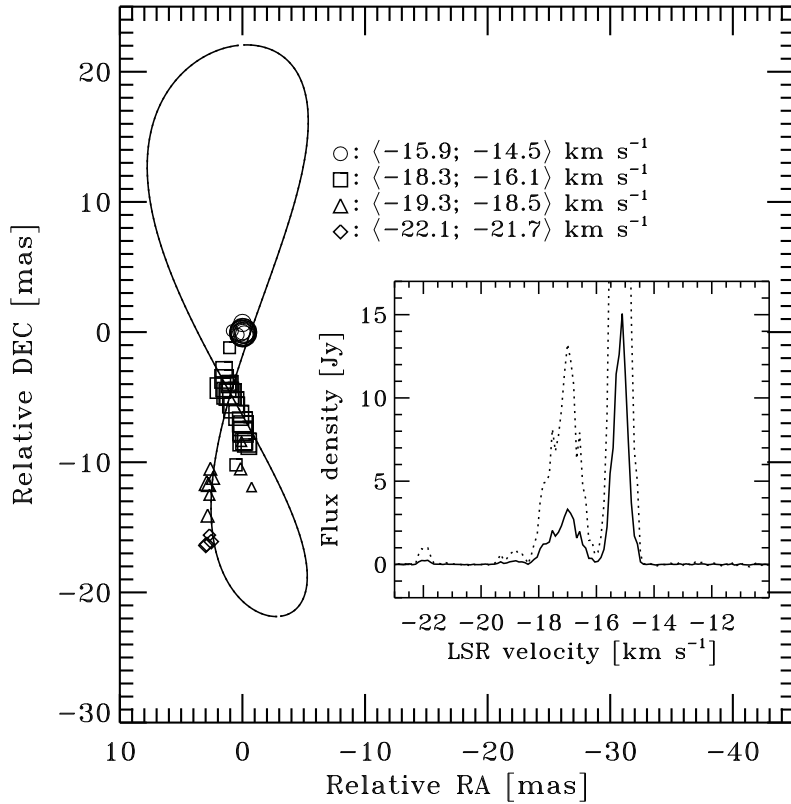


Figure 1. Water maser distribution observed towards V778 Cyg (Szczerba et al. 2006). The coordinates are measured relative to the position of the strongest feature at -15 km s^{-1} at $(\alpha, \delta) = (20^{\text{h}}36^{\text{m}}07^{\text{s}}.38327, 60^{\circ}05'26''.024)$. The solid curve shows the best fit to a model of a doubly-warped ring of radius 40 AU (at the assumed distance of 1.8 kpc) which is thin in the radial direction; other parameters are presented in Table 1. The ring centre is at the origin of the coordinate system. The insert shows the MERLIN spectrum of the H_2O maser emission. The dotted curve shows the spectrum magnified by a factor of four to enlarge the weak features.

2 DATA

The silicate carbon star V778 Cyg is located at a distance of about $d = 1.8 \text{ kpc}$, while the carbon star luminosity is $L_* \approx 5.6 \cdot 10^3 L_{\odot}$ (Benson & Little-Marenin 1996). Observations of V778 Cyg at 22 GHz by MERLIN revealed that the water maser features form an S-shaped structure with an angular size of 18 mas (Szczerba et al. 2006; see Fig. 1). The observed line-of-sight velocities of masing blobs depend almost linearly on the impact parameter measured along the major axis of the structure as shown in Fig. 2. The total spectrum of water maser emission (see insert in Fig. 1) consists of four major components near -22 , -19 , -17 and -15 km s^{-1} . The last component is the strongest, with a central peak of about 15 Jy, which corresponds to a lower limit to the brightness temperature of $T_b = 6 \cdot 10^8 \text{ K}$ (Szczerba et al. 2006).

3 MODELLING

Szczerba et al. (2006) show that the structure and velocity field of the maser features (presented in Figs. 1 and 2) are consistent with a Keplerian disc, observed almost edge-on, and present a simple quantitative interpretation of the observational data. The three maser spectral components at -19 , -17 , and -15 km s^{-1} (see Fig. 1) have been detected in every observation during the whole period from 1988 to 2002. They are symmetric around -17 km s^{-1} in velocity space. They are also almost equally displaced on the sky. By analogy with water masers in AGNs, this has prompted the interpretation that these are the systemic and the high velocity components that appear towards the centre and in the wings of a Keplerian disc (see e.g. Miyoshi et al. 1995; Bragg et al. 2000). In that case the velocities of the individual features making up the systemic

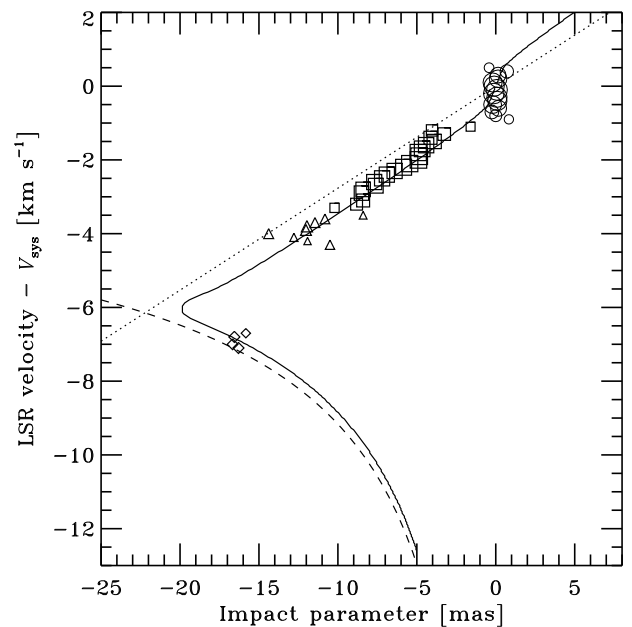


Figure 2. Dependence of the velocities of the maser features on the impact parameter measured along the major axis of the observed structure, relative to the brightest feature at -15 km s^{-1} , which is assumed to be the systemic velocity V_{sys} . The solid curve represents the model velocity dependence corresponding to a Keplerian disc with the inner and outer radii of $R_{\text{in}} = 10$ and $R_{\text{out}} = 40 \text{ AU}$, with $V(b)$ computed from $\partial\tau_m/\partial b = 0$, where τ_m is given by Eq. (1). The linear dependence $V(b) = V_K(R_{\text{out}})b/R_{\text{out}}$ is shown by a dotted line for comparison. The pure Keplerian rotation law $V(b) \propto 1/\sqrt{b}$ is shown by a dashed curve.

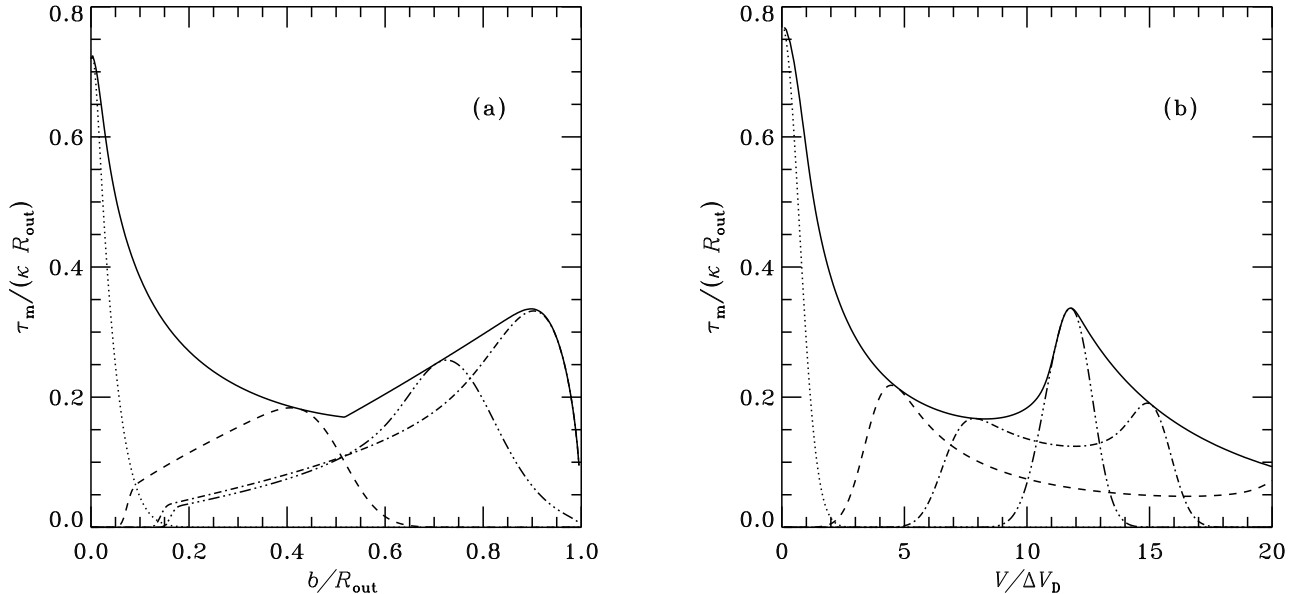


Figure 3. The optical depth in a maser line τ_m (in units κR_{out}) for $\xi = V_K(R_{\text{out}})/\Delta V_D = 11.7$ and the ratio of the inner-to-outer disc radii $R_{\text{in}}/R_{\text{out}} = 1/4$. The parameters are chosen to represent a disc around a $1.7M_\odot$ star, with the outer radius $R_{\text{out}} = 40$ AU and the gas temperature of 300 K. (a) Dependence on the impact parameter b for the velocities $V' = V/\Delta V_D = 0$ (dotted curve), 5.7 (dashed curve), 11.4 (dot-dashed curve), 13.3 (triple dot-dashed curve). (b) Dependence on the velocity of maser features for $b/R_{\text{out}} = 0$ (dotted curve), 0.3 (dashed curve), 0.6 (dot-dashed curve), 0.9 (triple dot-dashed curve). Solid curves show the maximum τ_m as a function of b and V (see Section 3.1).

component should show a linear dependence on the impact parameter $V(b) \propto b$ (Grinin & Grigor'ev 1983; Watson & Wyld 2000) which indeed is the case (see Fig. 2). This linear dependence could be interpreted as solid-body rotation. However, such an explanation is highly unlikely, because this requires a self-gravitating disc having a mass comparable to or even larger than the central mass. In such a case, the number density in the disc would be too high for the maser to operate as the population levels of water molecules would become thermalised by collisions with hydrogen.

On the other hand, the Keplerian disc interpretation implies a velocity at the outer radius of $V_K \approx 2 \text{ km s}^{-1}$ and a disc radius of $R \approx 11$ AU. The component at -22 km s^{-1} , which appeared in the spectrum in 1992, causes a problem for this model. It lies farthest from the disc centre but has too large a velocity for a simple Keplerian disc.

The S-shape is likely to result from the curving of the disc (Szczerba et al. 2006). However, the observed displacement of maser features at -19 km s^{-1} relative to those at $-17 \pm 1 \text{ km s}^{-1}$ is very large and is comparable to the estimated disc radius, which would be inconsistent with a simple model of a *slightly warped* masing disc, widely accepted, for example, for NGC 4258 (e.g. Miyoshi et al. 1995). The disc radius thus could be larger than the assumed 11 AU (corresponding to 6 mas), and the maser emission at -22 km s^{-1} could still come from the disc.

The stability of the dust spectrum (Y00) and of the water maser spectral features (Engels & Leinert 1994) prompts us to suggest that they have a common origin in the O-rich material in the disc. This disc is unlikely to be located around the carbon star, because the dust would be blown away by the stellar radiation at the distance corresponding to the observed disc size. It is thus natural to accept the hypothesis of Y00 and consider a disc around the companion of the carbon star in a binary system.

3.1 Masers from a Keplerian disc

Let us first consider a flat thin disc in Keplerian motion. The theory of masers from Keplerian discs is well developed (Grinin & Grigor'ev 1983; Watson & Wyld 2000). Masers are bright when the line of sight crosses the disc at a grazing angle, close to edge-on. Due to the velocity gradient, the maximum maser coherence length is reached towards the disc centre (where the matter moves perpendicular to the line of sight) and near the outer parts (where the gas motion is almost parallel to the line of sight). The strongest spectral features thus appear at the systemic velocity and at velocities shifted towards the red and blue by almost the Keplerian velocity near the outer edge of the masing disc.

The optical depth in a masing line, integrated along the line of sight s , as a function of the impact parameter b and velocity V is given by (see, for example, Grinin & Grigor'ev 1983; Watson & Wyld 2000)

$$\tau_m(b, V) = \int \kappa \exp \left\{ - \left(\frac{b \Omega_K(r) - V}{\Delta V_D} \right)^2 \right\} ds, \quad (1)$$

where κ is the maser opacity, $\Omega_K(r) = V_K(r)/r$ is the Keplerian angular velocity at radius $r = \sqrt{s^2 + b^2}$, $\Delta V_D = (2kT/m_{\text{H}_2\text{O}})^{1/2}$ is the thermal velocity for water molecules, and T is the gas temperature.

The upper integration limit $\sqrt{R_{\text{out}}^2 - b^2}$ is determined by the outer disc radius R_{out} . The lower limit is either zero or $\sqrt{R_{\text{in}}^2 - b^2}$ (corresponding to the inner disc radius R_{in}). Equation (1) gives half of the total optical depth along the line of sight. The optical depth can be expressed as a function of dimensionless variables $b' = b/R_{\text{out}}$ and $V' = V/\Delta V_D$:

$$\frac{\tau_m(b', V')}{R_{\text{out}}} = \int \kappa \exp \left\{ - \left(\frac{\xi b'}{r'^{3/2}} - V' \right)^2 \right\} ds', \quad (2)$$

Table 1. Model parameters

| R_{out}^a AU | i^b deg | Φ^c deg | Θ^d deg | A^e | V_{sys}^f km s $^{-1}$ | M_s^g M_\odot |
|--------------------------|--------------|-----------------|-------------------|-----------------|------------------------------------|----------------------|
| 40 ± 3 | 84.5 ± 1 | -8 ± 2 | 4 ± 2 | 0.23 ± 0.01 | -15 | 1.7 ± 0.1 |

^a The outer disc radius. ^b The inclination angle of the disc plane. ^c The phase angle (see eq. [3]). ^d The position angle of the line of nodes. ^e The amplitude of the shear wave (see eq. [3]). ^f Systemic velocity. ^g The mass of the companion.

where r' and s' are the corresponding distances measured in units of R_{out} , and $\xi = V_K(R_{\text{out}})/\Delta V_D$ is the ratio of the Keplerian velocity at the outer disc edge to the thermal velocity. At constant opacity κ and temperature T , the integral in Eq. (2) depends only on ξ and on the disc geometry expressed through the ratio of the inner to the outer disc radii $R_{\text{in}}/R_{\text{out}}$.

Fig. 3 shows the dependence of the optical depth in a masing line τ_m on the impact parameter b and on the maser velocity V (the figure is identical if we substitute $v' \rightarrow -v', b' \rightarrow -b'$). Panel (b) shows that τ_m as a function of velocity has two peaks: near zero (systemic) velocity, where the impact parameter $b \sim 0$, and near the Keplerian velocity at the outer disc radius $V' \approx \xi$. In the latter case the dominant rays emerge at an impact parameter $b \approx 0.9R_{\text{out}}$ (for $\xi = 11.7$, which is considered here for application to V778 Cyg). In general, for a fixed b , the velocity spectrum has two maxima: one corresponds to almost solid-body rotation with $V(b) \approx V_K(R_{\text{out}})b/R_{\text{out}}$, another corresponds to the Keplerian rotation with $V(b) \approx V_K(b)$. The first one is much stronger at small impact parameters, while the latter dominates at larger b .

For a given velocity V , the optical depth as a function of the impact parameter b has a single maximum, as in Fig. 3(a). If emission at any given velocity is only detected at a single spatial position (e.g. Szczerba et al. 2006), $V(b)$ can be evaluated by fixing V and finding the value of b for which τ_m reaches the maximum, i.e. by solving the equation $\partial\tau_m/\partial b = 0$. This gives the relationship shown by the solid curve in Fig. 2. It has a solid-body rotation part at small b and a Keplerian part at large b . We also note that $V(b)$ is almost independent of ξ and $R_{\text{in}}/R_{\text{out}}$.

3.2 Disc geometry

The longest maser amplification length is reached when radiation passes through the main body of the disc or through its outer parts. The strongest spectral line for Keplerian discs (with small ratio of inner-to-outer radii) observed edge-on appears at the systemic velocity and its spatial position coincides with the projection of the disc centre. We therefore associate the strongest component in the observed maser spectrum of V778 Cyg (chosen as the origin of coordinates in Fig. 1) with the systemic component coinciding with the projection of the disc centre and fix the systemic velocity V_{sys} at -15 km s^{-1} , which is consistent with a value of V_{sys} obtained from the observations of OH masers (-15.7 km s^{-1} , Little-Marenin et al. 1988; -15.1 km s^{-1} , Barnbaum et al. 1991). We also expect to see strong maser features near the projection of the outer radius of the masing disc at velocities shifted from V_{sys} by the Keplerian velocity at this radius.

We would like to describe the positions of all maser features (Fig. 1) and their velocities (Fig. 2) simultaneously. We assume that

the masers are produced in a thin curved disc of a shape described by the following expression

$$z(R, \phi) = A(R) R \sin[m(\phi - \Phi)], \quad (3)$$

where R is the cylindrical radius, ϕ is the azimuthal angle and z is the deviation from the plane XY , where the Z -axis is chosen in the direction of the disc angular velocity. A is the amplitude of the shear wave (which we assume to be constant), and m and Φ are its azimuthal number and phase, respectively. The projection of the disc on the sky depends on the inclination angle i (the angle between the line of sight and the Z -axis) and on the position angle of the line of nodes Θ .

Theoretically, it is rather easy to produce a warp with azimuthal number $m = 1$ in a disc in a binary system, using tidal effects. The theory of such discs is quite well developed (see, for example, Papaloizou & Terquem 1995, and references therein). In that case, rings at different radii can have different inclination angles and the observed spatial distribution in Fig. 1 could be reproduced by two such rings: one ring of a larger radius reproduces maser features at velocities $V \gtrsim -15.9 \text{ km s}^{-1}$ and $V \lesssim -18.5 \text{ km s}^{-1}$, while another ring of a smaller radius produces features at $-18.3 \text{ km s}^{-1} \lesssim V \lesssim -16 \text{ km s}^{-1}$. However, the observed linear increase of maser velocities with the impact parameter means that all maser features lie on very close orbits. This makes the $m = 1$ warp interpretation improbable.

On the other hand, we find that the observed \mathcal{S} -like structure can be well described by a single orbit with azimuthal mode $m = 2$. We discuss possible reasons for origin of such warp in Section 4.2. We fit the spatial distribution of maser features and obtain the set of parameters which are given in Table 1 (parameters $R = R_{\text{out}}$, i , Φ , Θ and A). For illustration we present a three-dimensional image of the disc taking $R_{\text{out}} = R = 40 \text{ AU}$, assuming that A is constant and $R_{\text{in}} = 10 \text{ AU}$, in Fig. 4(a). At large impact parameters the coherent length for maser amplification is large in case of the flat disc. For the warped disc shown in Figure 4, the line of sight passes through a large portion of the disc at large negative values of X , and the maser is bright. However, at large positive X (see the extreme dotted curve in Fig. 4b corresponding to $X = 15 \text{ mas}$) it crosses the disc plane at a steep angle reducing thus the amplification length. At small negative X (see the thick solid curve 2), the line of sight passes through the whole disc, while at small positive X (dotted curves) it passes through one part of the disc only. This would explain why we only detect masers from one side of the disc. We explain this more fully in the next Section.

3.3 Maser velocity distribution

In a doubly-warped disc with $m = 2$, the velocities are not precisely described by the Keplerian rotation law. However, because the warp is not very large, we neglect possible deviations from Keplerian motion. To describe the velocity distribution of maser features, we fit the central mass M_s , while keeping all other parameters fixed at the values deduced from the geometry in Sect. 3.2.

In Section 3.2, we showed that the observed dependence of the velocity on the impact parameter can be well described by a theoretical $V(b)$ dependence for a Keplerian disc with $M_s = 1.7 M_\odot$ and other parameters from Table 1 (see solid curve in Fig. 2). In our interpretation the strongest maser feature at -15 km s^{-1} coincides with the systemic velocity (gas moving perpendicularly to the line of sight) and is projected towards the disc centre $b = 0$. The features at $\approx -17 \text{ km s}^{-1}$ (i.e. -2 km s^{-1} on Fig. 2) corresponding to the impact parameter $b \approx 0.2R_{\text{out}}$ show a linear dependence close to

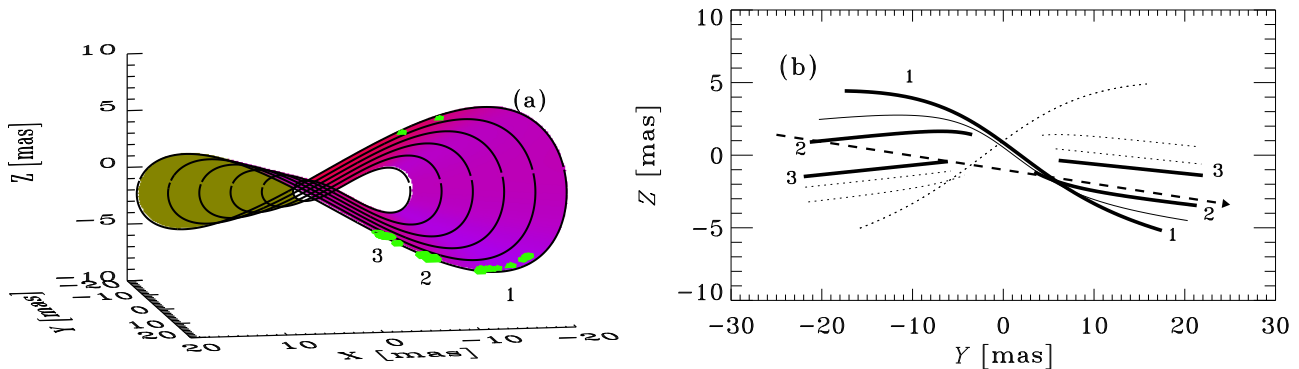


Figure 4. (a) Three-dimensional image of the mid-plane of the masing disc with $m = 2$ and of the maser spots in V778 Cyg. The line of sight lies in the YZ plane and makes an angle of 5.5° with the Y -axis. The coordinates of the disc centre are $(0,0,0)$. The grey (green) spots show positions of masers. (b) Cross-sections of the disc mid-plane for $X = -13, -8, -5, 0, 2, 4, 15$ mas. Solid and dotted curves correspond to negative and positive values of X . The strongest masers at $-22, -17$ and -15 km s^{-1} appearing at $X \approx -13, -5$ and 0 are shown as spots in panel (a) and marked by 1, 2 and 3, respectively. The disc cross-sections are these X are shown by thick solid curves in panel (b). The dashed line with an arrow shows the line of sight.

$V(b) \approx V_K(R_{\text{out}})b/R_{\text{out}}$ (shown by the dotted line). If the disc were flat, these features would be weaker than the systemic feature at $b = 0$, because the optical depth at this position is about 40 per cent of that at $b = 0$ for the assumed gas temperature $T = 300$ K (see Fig. 3). However, because of the warping, the line of sight at $b \approx 0.2R_{\text{out}}$ passes almost through the whole disc (see curve 2 on Fig. 4(b)), whereas the amplification at $b = 0$ takes place through only half of the disc (again because of the warp). This results in a strong increase of the maser power at these intermediate velocities and impact parameters.

The weakest detected component at -22 km s^{-1} (i.e. -7 km s^{-1} in Fig. 2) lies exactly at the velocity-impact parameter relationship computed for a Keplerian disc, which at large b follows a simple Keplerian rotation law $V(b) \propto 1/\sqrt{b}$ (the dashed curve in Fig. 2). The position and velocity of this component are consistent with the expected theoretical peak of the maser emission at $b \approx 0.9R_{\text{out}}$ and $V \approx V_K(R_{\text{out}})$ (see Fig. 3).

We now note that for a flat, symmetric disc both blue-shifted and red-shifted components should be observed around the systemic velocity. However, only blue-shifted features are visible (Fig. 1). In a warped disc the line of sight cuts the near and far sides of the disc at different angles. The cross-sections of the central disc plane are shown in Fig. 4(b). The solid and dotted curves correspond to the projections where the maser amplification would give the blue- and the red-shifted components, respectively. It is clear from the discussion in the previous section that the amplification lengths for the blue-shifted maser components are larger, which would explain the absence of the red-shifted components in the maser spectrum.

3.4 Dust emission

The infrared spectrum of V778 Cyg obtained by *ISO/SWS* and *IRAS/LRS* shows strong silicate features at 10 and 18 μm (see Fig. 5 and Y00). The silicate features as well as the water maser features are very stable (Y00; Engels & Leinert 1994), so it is natural to assume that the dust and water are co-spatial, as we can show that similar conditions can explain the observations. Both can then be located around the companion in disc, which could have been formed while presently C-rich star was still O-rich, and as a result, it contains the O-rich dust and gas which is responsible for the observed

O-bearing dust/molecule features. However, a small amount of carbon rich dust from the later stellar wind could also have been captured by the companion. We therefore assume that both astronomical silicate and amorphous carbon grains are present in the masing disc.

We assume that the dust is optically thin and is heated by the carbon star of radius $R_* = 2$ AU and temperature of $T_* = 2400$ K (Engels & Leinert 1994; Benson & Little-Marenin 1996). The heating of the dust by the companion is negligible if it is a main sequence star. The fitting parameters are the dilution factor W , the mass of dust, and the dust grain size a . We find that the data are best described for $a = 0.5$ μm . Note, that it is larger than the typically assumed grain size of 0.1 μm in the envelopes of AGB stars (see e.g. Jura 1996; Groenewegen 2006). On the other hand, it seems reasonable that grains would grow whilst in a disc (see Lissauer et al. 1996; Jura et al. 2001; D'Alessio et al. 2006; Dent et al. 2006), whereas the smallest grains would be blown away by the carbon star radiation (see Section 4.1). The observed IR spectrum is well described (see Fig. 5) by a model with $W = 1.6 \cdot 10^{-4}$ for $M_{\text{as}} = 5.6 \cdot 10^{-7} M_\odot$ of astronomical silicate and $M_{\text{ac}} = 6.7 \cdot 10^{-8} M_\odot$ of amorphous carbon (with corresponding temperatures of $T_{\text{as}} = 290$ K and $T_{\text{ac}} = 470$ K obtained from the energy balance). The distance between the carbon star and the dust material can thus be estimated from the dilution factor: $D = 0.5W^{-1/2}R_* \approx 80$ AU.

3.5 Maser pumping model

As we argued above, the observed emission of the $6_{16} - 5_{23}$ maser at 22 GHz most probably originates in the disc around the companion to the carbon star. The hydrogen and water vapor in the disc are probably mixed with the amorphous carbon and astronomical silicate dust grains. We assume a solar abundance of elements, giving a water-to-gas mass ratio of $f_{\text{H}_2\text{O}} = 6 \cdot 10^{-3}$ (see, for example, Jeong et al. 2003). The maser strength depends on the hydrogen number density n_{H_2} , water fraction $f_{\text{H}_2\text{O}}$ and the dust-to-gas mass ratio f_d as well as on the gas and dust temperatures.

The dust temperature is determined from heating by the carbon star and cooling by its own radiation (see Sect. 3.4). The gas temperature is determined by collisions with the dust grains and radiative cooling by water molecules. We take $n_{\text{H}_2} = 10^8$ cm^{-3} (Kylafis & Norman 1991) and use $f_d = 10^{-2}$ (Yamamura et al. 2000), a typical ratio in circumstellar envelopes, everywhere in the

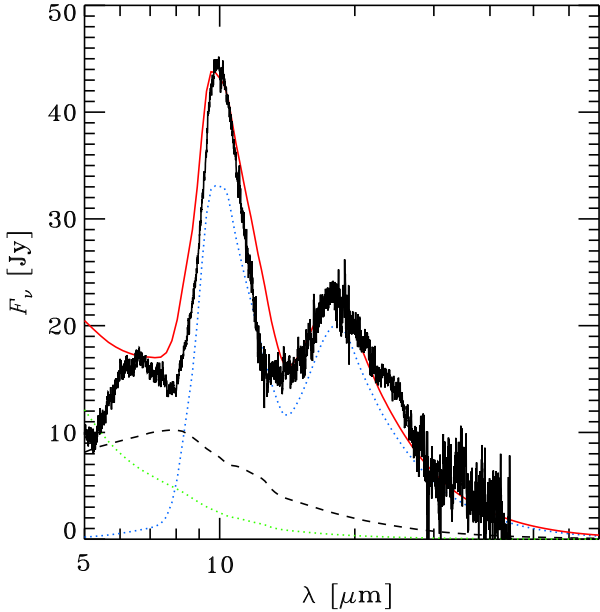


Figure 5. The silicate emission bands in the spectra of V778 Cyg observed by *ISO/SWS* and *IRAS/LRS* (Y00). The blue dotted and black dashed curves refer to astronomical silicate and amorphous carbon model spectra, respectively. The dot-dashed curve corresponds to the 2400 K black body emission of the carbon star. The red solid curve shows the total model spectrum.

masing disc. We justify our choice of these parameter values in Sect. 4.1. Solving the energy balance for the gas, we find $T \approx 300$ K at the disc mid-plane. We assume the same temperature throughout the disc.

The conditions in the disc are within the range giving rise to collisionally-radiatively pumped, unsaturated maser emission. In order to estimate the maser power, we solve simultaneously the radiative transfer and statistical balance equations for the first 45 rotational levels of the ground and (010) excited vibrational levels of ortho- H_2O . We employ the escape probability method in order to solve the radiative transfer equation (for details, see Babkovskaia & Poutanen 2004, 2006). For a disc half-thickness of $H \sim 10^{14}$ cm at the outer disc edge (obtained by considering the conditions for hydrostatic equilibrium, see below), we obtain a maser absorption coefficient of $\kappa = -4.5 \cdot 10^{-14} \text{ cm}^{-1}$. This gives the maximum maser optical depth $\tau_m \approx 0.73 \kappa R_{\text{out}} \approx -20$ along the line of sight at the disc mid-plane in the direction of the maser component at the systemic velocity (see Fig. 3), assuming that amplification takes place only on one side of the disc. The corresponding maximum brightness temperature is $T_b = -T_{\text{ex}} \exp(-\tau_m) = 5 \cdot 10^{10}$ K, for an excitation temperature $T_{\text{ex}} = -100$ K. Averaging the brightness temperature over the disc height we get $T_b \approx 1.5 \cdot 10^{10}$ K. This is above the lower limit of $6 \cdot 10^8$ K imposed by the observational data. Thus, the conditions in the disc can easily reproduce the observed strength of the maser emission.

4 DISCUSSION

4.1 Disc stability

From the IR spectrum, we have estimated a distance of ~ 80 AU between the carbon star and the region containing the dust. This separation is consistent with the scenario in which the dust has

been captured in a disc around a (probably main-sequence) companion (Y00). Moreover, this estimate is just above the lower limit constrained by the velocity stability of the maser spectral features (Szczerba et al. 2006). We estimated the radius of the masing disc to be about 40 AU by fitting the spatial distribution of masers (Table 1). This is also consistent with the observed velocity profile.

For the disc to be stable, its radius should certainly be smaller than the distance from the companion to the inner Lagrangian point, which is about 44 AU, for the assumed mass of the carbon star of about $1M_{\odot}$ (Y00) and the companion mass of $M_s = 1.7M_{\odot}$.

The stability of the disc also puts constraints on the dust-to-gas mass ratio f_d . The radiation pressure F_{rad} from the carbon star acting on the dust should be balanced by the gravitational force F_{grav} due to the companion acting on the gas:

$$\frac{F_{\text{rad}}}{F_{\text{grav}}} = \left(\frac{L_*}{4\pi D^2} \frac{\pi a^2 Q}{c} \right) \left(\frac{GM_s}{R^2} \frac{4\pi a^3 \rho_d}{3f_d} \right)^{-1} < 1, \quad (4)$$

where $Q \approx 0.2$ is the extinction efficiency of the dust (see Ossenkopf et al. 1992) and $\rho_d \approx 3 \text{ g cm}^{-3}$ is the dust density. For a disc radius of $R = 40$ AU, equation (4) gives $f_d \lesssim 0.02$.

We use the total dust mass in the disc $M_{\text{dust}} = M_{\text{as}} + M_{\text{ac}} = 5.7 \cdot 10^{-7} M_{\odot}$ to provide an estimate of the hydrogen number density assuming a homogeneous isothermal disc:

$$n_{\text{H}_2} = \frac{M_{\text{dust}}}{f_d V_{\text{disc}} m_{\text{H}_2}} \gtrsim 5 \cdot 10^7 (T/300 \text{ K})^{-1/2} \text{ cm}^{-3}, \quad (5)$$

where $V_{\text{disc}} \approx 4HR_{\text{out}}^2$ is the disc volume, $H = R_{\text{out}} V_t / V_K(R) \approx 10^{14}$ cm is the disc half-thickness (assuming hydrostatic equilibrium), $V_t \approx 1.5(T/300 \text{ K})^{1/2} \text{ km s}^{-1}$ is the gas thermal velocity, $V_K = 6.1 \text{ km s}^{-1}$ is the Keplerian velocity at the outer disc radius $R_{\text{out}} = 40$ AU and m_{H_2} is the mass of hydrogen molecule. An additional condition for disc stability is the requirement that the radiation pressure must be smaller than the rate of momentum exchange between the grains and the hydrogen molecules, giving another constraint on n_{H_2} :

$$F_{\text{rad}} \lesssim m_{\text{H}_2} V_t / t_{\text{coll}} \approx m_{\text{H}_2} V_t^2 n_{\text{H}_2} \pi a^2, \quad (6)$$

where t_{coll} is the typical time between grain-molecule collisions. We obtain $n_{\text{H}_2} \gtrsim 5 \cdot 10^7 \text{ cm}^{-3}$, which is in perfect agreement with Eq. (5). This justifies our choice of $n_{\text{H}_2} = 10^8 \text{ cm}^{-3}$ and $f_d = 10^{-2}$ when estimating the maser power in Sect. 3.5.

4.2 Origin of a disc with $m = 2$

We note that at the present time there is no theoretical description of how to produce an $m = 2$ warped disc (see, however, Lubow & Ogilvie 2000, and reference therein). An $m = 2$ warp might be induced by a non-linear development of warping instabilities due to the tidal forces from the companion (Lubow 1992; Lubow & Ogilvie 2000). The $m = 1$ warping results in density waves described by the azimuthal mode $m = 2$ (Papaloizou & Terquem 1995). The effect of radiation pressure (Pringle 1996) on these waves can produce an $m = 2$ warp. Such $m = 2$ warps cannot realistically have an amplitude A larger than the disc dimensionless half-thickness H/R . Assuming hydrostatic equilibrium in the disc, we can estimate the ratio $H/R = V_t / V_K(R) \approx 0.24$, which is of the same order as the value of $A \approx 0.23$ which we obtain (see Table 1). More theoretical work is required to address the possibilities of $m = 2$ warps properly.

5 CONCLUSIONS

MERLIN imaging of water masers from the silicate carbon star V778 Cyg show clear evidence that they arise from a disc around a companion to the carbon star. We estimate the mass of the companion to be $\sim 1.7 M_{\odot}$ and the distance between the stars to be ~ 80 AU. This is independently confirmed by the stability over time of the velocity of the major maser spectral features. The radius of the masing disc is about 40 AU. We develop a model for the disc which is consistent with all available observational constraints.

The silicate dust, observed in the infrared by *ISO* and *IRAS*, is likely to be co-spatial with the water vapor producing the maser emission. This O-rich material must have originated during an earlier phase of the carbon star and has been captured in a disc around the companion. The carbon star is about a thousand times more luminous than its companion and is the major source of heating in the system.

We find that the observed spectrum of dust radiation is well described by a combination of $0.5\mu\text{m}$ astronomical silicate and amorphous carbon grains, with masses $M_{\text{as}} = 5.6 \cdot 10^{-7} M_{\odot}$ and $M_{\text{ac}} = 6.7 \cdot 10^{-8} M_{\odot}$. We model the conditions necessary for a stable disc, which constrain the dust-to-gas mass ratio to be $f_d \lesssim 0.02$ and the hydrogen number density to be $n_{\text{H}_2} \gtrsim 5 \cdot 10^7 \text{ cm}^{-3}$. The dust temperatures of $T_{\text{as}} = 290$ K and $T_{\text{ac}} = 470$ K, obtained from the energy balance, yield gas temperature around 300 K (determined by collisions with the dust grains and radiative cooling by water molecules). These conditions at the same time predict very effective water masing and show that the masers could reach a brightness temperature more than an order of magnitude larger than the lower limit, obtained from the observational data.

The observed maser geometry and velocity distribution are consistent with a doubly-warped Keplerian disc, described by the azimuthal mode $m = 2$. We find that the thickness of the disc and the warp amplitude of our model are also consistent with the demands of hydrostatic equilibrium. We predict successfully the asymmetric appearance of the disc and explain the origin of the various maser components. At present, the theory of such $m = 2$ discs is absent, and this could be an interesting challenge for future theoretical studies.

ACKNOWLEDGMENTS

This work was supported by the Finnish Graduate School for Astronomy and Space Physics, the Magnus Ehrnrooth Foundation (NB), and by the grant 2.P03D017.25 of the Polish State Committee for Scientific Research (RS). We are grateful to I. Yamamura for providing the IR spectrum of V778 Cyg and P. Ivanov for his help in interpretation of the warped disc. We thank the referee for useful suggestions.

REFERENCES

Babkovskaia N., Poutanen J., 2004, *A&A*, 418, 117
 Babkovskaia N., Poutanen J., 2006, *A&A*, 447, 949
 Barnbaum C., Kastner J. H., Morris M., Likkell L., 1991, *A&A*, 251, 79
 Benson P. J., Little-Marenin I. R., 1996, *ApJ*, 106, 579
 Bragg A. E., Greenhill L. J., Moran J. M., Henkel C., 2000, *ApJ*, 535, 73
 Chen P., Wang X., Wang F., 1999, *ChA&A*, 23, 371

D'Alessio P., Calvet N., Hartmann L., Franco-Hernández R., Servín H., 2006, *ApJ*, 638, 314
 Dent W. R. F., Torrelles J. M., Osorio M., Calvet N., Anglada G., 2006, *MNRAS*, 365, 1283
 Engels D., Leinert C., 1994, *A&A*, 282, 858
 Evans T. L., 1990, *MNRAS*, 243, 336
 Grinin V. P., Grigor'ev S. A., 1983, *Sov. Astr.*, 27, 298
 Groenewegen M. A. T., 2006, *A&A*, 448, 181
 Jeong K. S., Winters J. M., Le Bertre T., Sedlmayr E., 2003, *A&A*, 407, 191
 Jura M., 1996, *ApJ*, 472, 806
 Jura M., Webb R. A., Kahane C., 2001, *ApJ*, 550, L71
 Kylafis N. D., Norman C., 1991, *ApJ*, 373, 525
 Lissauer J. J., Wolk S. J., Griffith C. A., Backman D. E., 1996, *ApJ*, 465, 371
 Little-Marenin I. R., 1986, *ApJ*, 307, L15
 Little-Marenin I. R., Benson P. J., Dickinson D. F., 1988, *ApJ*, 330, 828
 Lubow S. H., 1992, *ApJ*, 398, 525
 Lubow S. H., Ogilvie G. I., 2000, *ApJ*, 538, 326
 Miyoshi M., Moran J., Herrnstein J., Greenhill L., Nakai N., Diamond P., Inoue M., 1995, *Nature*, 373, 127
 Morris M., Guilloteau S., Lucas R., Omont A., 1987, *ApJ*, 321, 888
 Ossenkopf V., Henning T., Mathis J. S., 1992, *A&A*, 261, 567
 Papaloizou J. C. B., Terquem C., 1995, *MNRAS*, 274, 987
 Pringle J. E., 1996, *MNRAS*, 281, 357
 Szczerba R., 2002, *Adv. Space Research*, 30, 1979
 Szczerba R., Szymczak M., Babkovskaia N., Poutanen J., Richards A. M. S., Groenewegen M. A. T., 2006, *A&A*, in press [astro-ph/0504354]
 Watson W. D., Wyld H. W., 2000, *ApJ*, 530, 207
 Yamamura I., Dominik C., de Jong T., Waters L. B. F. M., Molster F. J., 2000, *A&A*, 363, 629